COLLOID SCIENCE

Electrokinetic potentials at the gas-aqueous interface by spinning cylinder electrophoresis

Julie A. McShea and I. C. Callaghan

BP Research Centre, Middlesex, UK

Abstract: The natural buoyancy of gas bubbles has hampered conventional electrokinetic methods of evaluating charge at the gas-liquid interface.
In this study, bubbles are held by centripetal force at the centre of a horizontal, rotating cylinder filled completely with liquid. Migration of the bubble along the axis of the cylinder can be achieved by applying a gravity force or an electrophoretic force.
An expression for the drag coefficient has been developed and used to calculate surface charge densities and electrokinetic potentials. In the presence of potassium chloride, anionic and non-ionic surfactants, the electrokinetic potentials were negative (~2–5 mV) at the air-aqueous interface. A cationic surfactant rendered the zeta potential positive.
A knowledge of the air-aqueous interfacial rheology is desirable if the drag coefficient, and consequently the zeta potential, at all types of gas-liquid interfaces is to be evaluated.

Key words: Electrokinetic potential, gas-aqueous interface, spinning cylinder.

1. Introduction

The possibility of a charge arising at the gas-aqueous interface and subsequent evaluation of that charge is of interest to many colloid chemists. It is particularly relevant to the process of mineral recovery by flotation.

Zeta potentials at solid-liquid interfaces have been investigated widely by conventional micro-electrophoresis, but due to the natural buoyancy of gas bubbles, these techniques cannot be adapted easily for studies at the gas-liquid interface.

Several different approaches have been adopted to measure this charge [1–3], but all have associated problems. The majority of workers have chosen the spinning cylinder technique, where the bubble moves along the axis of a horizontal, spinning, closed cylinder. This method is relatively simple to set-up, but interpretation of the results is difficult in the absence of a hydrodynamic treatment of the drag forces encountered by the bubble.

In this paper, the movement of bubbles due to gravity and electrophoretic forces at much slower angular speeds than hitherto employed, is described. Electrophoretic velocity measurements, taken over a range of pH values and in the presence of various surfactants are presented. An expression for the drag forces on the moving bubble has been developed, allowing the potential at (or near) the air-aqueous interface to be calculated.

2. Theory

2.1 Origin of a charge at the gas-liquid interface

It is clear that ionic surfactants adsorb at the gas-aqueous solution interface and give rise to a surface charge; however, the formation of a charged interface in the presence of simple ions or in distilled water is more difficult to postulate. Negative potentials at hydrocarbon-aqueous and air-aqueous interfaces in simple salt solutions or distilled water have been widely reported [4]. It has been suggested that, in the case of electrolytes, negative adsorption of cations occurs, giving rise to a charge separation, and for distilled water, that dipole orientation is responsible for the electrial potential.

2.2 Forces on a bubble in a rotating cell

Movement of a bubble along the axis of a rotating cell may be induced by a gravitational force and/or an electrophoretic force. For the velocity to remain constant, i.e. no acceleration, the force causing the movement must be balanced by equal and opposite

retarding forces. A full treatment of the drag forces is not available, although factors affecting the magnitude of these forces have been recognised by some workers, notably Whybrew [3] and Huddleston and Smith [4]. Three forces on the bubble are immediately apparent:

(a) A centripetal force due to spinning of the cylinder;

(b) Gravity;

(c) A viscous drag force.

Hydrodynamicists, in particular Stewartson [5] and Hocking et al. [6], have proposed equations and models for a spinning bubble moving axially in an inviscid fluid. Batchelor [7] recognised that other important forces acting on the bubble are the Coriolis forces. Rotation confers a degree of elasticity to the rotating liquid which provides a restoring mechanism allowing the propagation of waves through the liquid. The Coriolis forces are directed at a right angle to the axis of rotation and local velocity direction. They act in a restoring sense and do no work on the body. More simply, the Coriolis forces tend to oppose the motion of a bubble along the axis and pull it back towards the plane of rotation. If the rotation is anti-clockwise the restoring movement of the bubble relative to the rotating cylinder is clockwise (see fig. 1 for a pictorial presentation of the forces experienced by the bubble).

The Rossby number (Ro) defined by:

$$Ro = \frac{u}{2\,a\,\Omega} \tag{1}$$

where u = velocity of bubble, a = radius of bubble, Ω = angular speed of rotation

is a measure of the relative importance of the effects of movement of a body and rotation of the fluid. As Ro tends to zero it is reasonable to suppose that inertial forces are small compared with Coriolis forces. In this regime ($Ro < 0.3$) Taylor [8] showed that the sphere carries with it a long column of liquid whose axis is parallel to the rotation axis. Where Ro is approximately one the magnitude of the inertial and Coriolis forces are comparable and axisymmetric waves in the fluid, extending to infinity, are liable to be produced.

Currie and Nieuwkoop [9] described the fluid layers around a spinning drop viz: layers of liquid (Ekman layers) close to the drop which rotate rigidly with it, and a free shear layer which is bounded by the liquid layer close to the drop and the bulk of the liquid rotating with the cylinder. The shear free layer defines the edge of the Taylor column and Currie and Nieuwkoop produced photographic evidence for a spiral-like flow pattern within the layer.

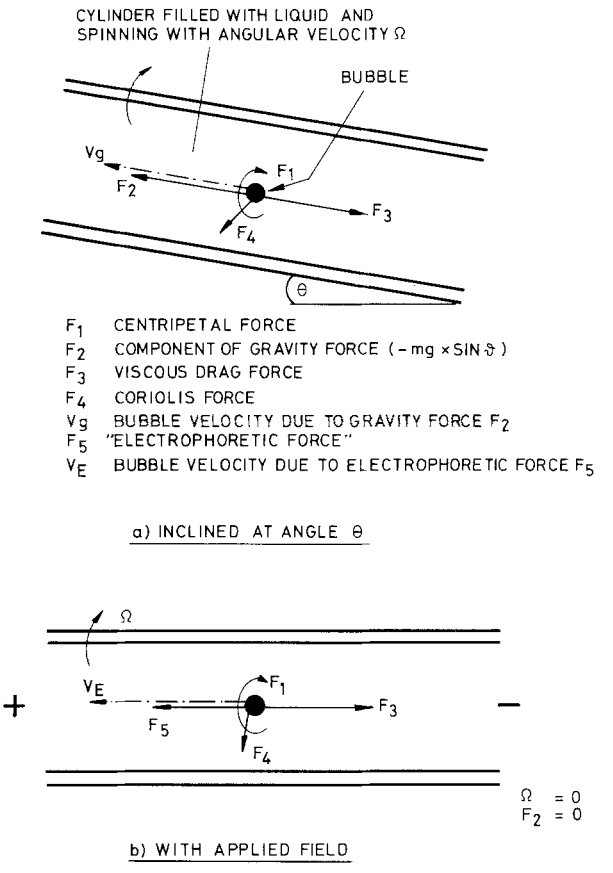

Fig. 1. Forces acting upon bubble in the spinning cylinder

Viscosity effects of the liquid layers moving close to the boundary of the bubble may be neglected only if the Ekman number (E) is sufficiently small:

$$E = \frac{\mu}{\varrho\,\Omega_a 2} \tag{2}$$

where: μ = viscosity of surrounding fluid, ϱ = density of fluid.

The Taylor number is given by,

$$T = E^{-1} \tag{3}$$

The effect of the end caps upon the Taylor column and the overall drag has been investigated by Hocking [6]. A long cylinder is considered to be where δ is large, so that,

$$\delta = \frac{hE}{2a} \tag{4}$$

where: h = length of cylinder.

A short cylinder is considered to be where $h \leqslant aE^{-1}$.

For the cylinder, size of bubbles and rotation speeds used in this study, typical Rossby and Ekman numbers are: $Ro \sim 0.02$, $E \sim 0.4$ and $T \sim 2.5$, i.e. Coriolis forces are important and a Taylor column will develop. $\delta \sim 56$ and $aE^{-1} \sim 0.09$, therefore the cylinder is considered 'long', however, as there are strong, swirling motions inside the column but none outside, there should always be end effects.

The bubble was seen to adopt off-axis, stationary positions, i.e. the bubble rotated about itself, but not with the cylinder, depending upon the speed of rotation. This phenomenon was observed by Currie and Nieuwkoop and was attributed to an interplay between the buoyancy force tending to push the bubble upwards and the pressure forces (proportional to the rotation speed) encouraging the bubble to the centre.

Rallison [10] has considered that for an axisymmetric particle moving along the rotation axis, the force on the particle can be defined simply as:

$$F = Du \tag{5}$$

where: D = drag coefficient, dependent upon the Taylor number.

For small values of T, where the Coriolis forces are small, the flow is Stokesian and the drag coefficient, allowing for wall effects [18] is represented by:

$$D = \frac{6\,\Pi\mu a}{1 - \left(\frac{2.1a}{R}\right)} \tag{6}$$

where: R = radius of cylinder.

For larger values of T, as found in this study, the drag coefficient is determined as a function of T[10]:

$$D = \frac{16}{3}(\varrho - \varrho o)a^3\,\Omega\hat{D}(T) \tag{7}$$

where: ϱo = density of sphere.

As T tends to infinity, $\hat{D}$ tends to one, and as T tends to zero, $\hat{D}$ tends to $\frac{9\Pi}{8T}$.

For intermediate values of T, an approximate result for $\hat{D}$ is:

$$\hat{D} = \frac{9\Pi + 8T}{8T} = \frac{\Pi g \sin\theta}{4\Omega\mu}. \tag{8}$$

This value was found to approximate our experimental results.

The interfacial viscosity of the air-liquid interface also plays a major role in the hydrodynamics of the situation, as this can alter the degree of slip at the air-liquid boundary. A perfectly clean, non-rigid interface is unable to support an Ekman layer, consequently, the Taylor column ahead of the bubble no longer has length T but extends to the end caps. The drag coefficient is then greater [19]:

$$D = T^{1/2} \text{ as } T \to \infty\,. \tag{9}$$

Where surfactant is present, and, indeed, any impurities in the system (it is virtually impossible to obtain a completely clean air-aqueous interface experimentally), the interface becomes more rigid. The size of the air bubble is also known to affect the rigidity of the interface, the smaller the bubble the more rigid it becomes [11]. The value of D for large T values will lie between the rigid stress value (one) and the stress-free value ($T^{1/2}$).

It becomes evident that a knowledge of the interfacial rheology is required in order to estimate the correct drag coeffient for the particular system. Also, in any one measurement of bubble velocity, the air-aqueous interfacial tension, hence interfacial rheology is liable to change due to Marangoni effects; therefore, errors in measurements are inevitable. The bubble will experience different drag forces as the Taylor column approaches the cylinder end caps. Consequently, only the central area of cylinder may be used reliably for velocity measurements.

The magnitude of the rotational speeds employed was low (< 100 rads^{-1}) and did not cause bubble distortion. No corrections for bubble shape were considered necessary.

2.3 Electrophoresis

Electrophoresis may be defined as the movement of charged particles or drops suspended in a liquid under the influence of an applied electric field. Theories relating the observed particle velocity with the potential at a shearing plane some distance from the particle surface, are well-documented for static, conventional systems [12]. The standard equations may not be applied to spinning cylinder electrophoresis as the bubble is subjected to different retarding drag forces due to the rotation. The distribution of ions around particles is known to be deformed by the electric field in conventional electrophoresis. In the rotating system, the viscosity and thickness of the liquid layers at the air/liquid boundary (Ekman layers), will affect

flow round the bubble. It seems reasonable to suppose that this swirling motion (in conjunction with electric field deformation), could affect the continuity of the double layer or even remove it altogether. The observed bubble velocity could be related to the zeta potential at the shearing plane or to the potential at the outer Helmholtz plane.

For the electrophoresis experiments the cylinder was horizontal so that the only force moving the bubble was the applied electric field across the cell. The drag force could then be equated to the electrostatic force acting on the bubble:

$$Du = Q\frac{dV}{dx} \tag{10}$$

where: Q = bubble surface charge (C), $\frac{dV}{dx}$ = applied electric field gradient (Vm^{-1})

Considering the aforementioned hydrodynamics, estimation of the charge will depend upon the Ekman number and rheology of the air/liquid interface. In estimations of the total charge, Q, we have assumed that the air bubbles are rigid and that the value of $\hat{D}$ (T) can be calculated using equation (8) (or equation (17), see results). This assumption of bubble rigidity seems to hold for bubbles of diameter less than ca 1 mm [13].

Following Debye and Hückel [14], the following expression for Q can be written:

$$Q = a\varepsilon\varepsilon o(1 + \varkappa a)\zeta \tag{11}$$

where: a = bubble radius, ε, εo = relative and free space permittivities respectively, $\varkappa$ = Debye-Hückel reciprocal length, ζ = electrokinetic potential.

Equation (11) is valid provided $\zeta < 25$ mV.

Substituting for Q in equation (10):

$$\zeta(\text{mV}) = \frac{1000\,Du}{a\varepsilon\varepsilon o(1 + \varkappa a)(dV/dx)}. \tag{12}$$

Also:

$$\sigma_D = \frac{Q}{4\pi a^2} = \frac{Du}{4\Pi a^2(dV/dx)}. \tag{13}$$

Values for the charge density and electrokinetic potential of a bubble in various solution environments can be calculated from experimental data using equations (12) and (13). The results of such calculations are tabulated in table 1.

2.4 *Electro-osmosis*

Measurement of the electrophoretic mobility is complicated by the phenomenon of electro-osmosis. If the walls of a standard electrophoresis cell are charged relative to the liquid, upon application of an electric field there will be a streaming of liquid at the walls. As the system is closed there is a return flow through the centre of the cell. Thus, the observed velocity of any particles is the sum of the velocity due to the electrophoretic force and velocity due to movement of the liquid. The true electrophoretic velocity may be measured only at a position in the cell where there is no net flow due to electro-osmosis, i.e. at the stationary layers.

It is by no means certain how (or if) this phenomenon is manifest in the rotating cell. The return flow of liquid due to electro-osmosis in a rotating cell is likely to be opposed by liquid movement due to the rotation and the development of a Taylor column. Visual evidence of the existence of a Taylor column has been produced (see fig. 6–8). Huddleston [15] observed that rotation had a diminishing effect upon the magnitude of electro-osmotic flow. Cell wall electro-osmotic velocity (regardless of the sign of the cell wall charge), did not affect axial mobility of hollow glass spheres.

Considering these observations, it is tentatively suggested that electroosmotic flow is not manifest in the rotating cell, at least not of the order of magnitude observed in stationary cells.

3. Apparatus, method and materials

3.1 *Apparatus and method*

The cylinder employed (fig. 2) was of accurately bored glass 100 mm long and 15 mm internal diameter. The Teflon end caps were fitted with blackened, circular, platinum electrodes. In all experiments the cylinder was filled completely with liquid and one air bubble was introduced by a microsyringe via an end cap. Angular speeds of the cylinder were measured by a mechanical tachometer and the velocity of the bubble obtained by viewing through a binocular eye – piece fitted with a graticule, and timing the bubble progress with a stopwatch. The angle of inclination of the cylinder was adjusted by means of a micrometer screw on the levelling table. The electric field was applied across the cell by a continuously variable 0–100 V DC supply unit.

The field strength E was measured as for a conventional cell:

$$E = \frac{V}{l} \tag{14}$$

where: V = voltage applied, l = effective length of cylinder.

The effective length of the cylinder was found by measuring the resistance of the spinning cylinder when filled with standard salt solution of known conductivity. In this instance, l measured 83.3 mm; this value was not affected by the spinning of the cylinder.

3.2 Materials

A cationic surfactant:
Arquad C/50: $C_{12}H_{25}N^+(CH_3)_3Cl^-$
ex Akzo Chemie.
Anionic surfactants:
Sodium dodecyl sulphate: $C_{12}H_{25}OSO_3^-Na^+$
ex B.D.H.
Sodium oleate: $CH_3(CH_2)_7CH(CH_2)_7COO^-Na^+$.
A zwitterionic surfactant:
Empigen BB: $C_{12}H_{25}N^+(CH_3)_2CH_2COO^-$
ex Marchon.
A polyoxyalkylene/alkyl phenol surfactant:
Synperonic NPE 1800
ex ICI

Surfynol 104: $(CH_3)_2CH\,CH_2\underset{\underset{OH}{|}}{C}-C\equiv C-\underset{\underset{OH}{|}}{C}-CH_2-CH(CH_3)_2$
ex Air Products Inc.

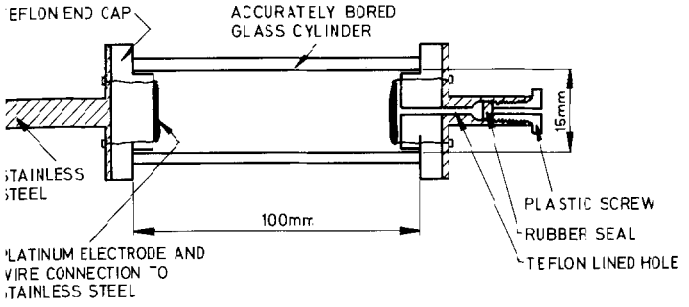

DETAIL OF THE CYLINDER AND END CAPS

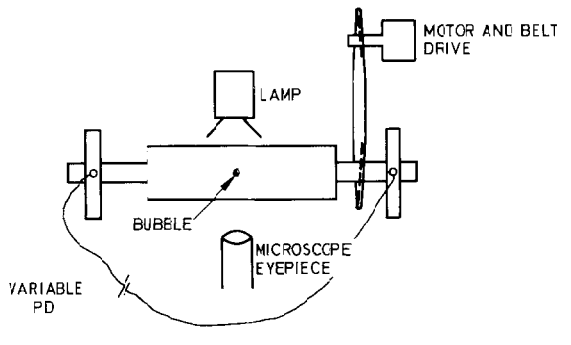

PLAN VIEW

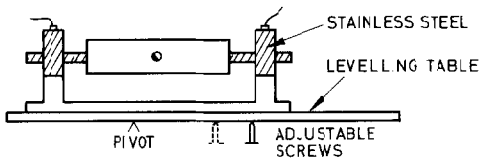

LATERAL VIEW

Fig. 2. The apparatus

Hollow glass spheres:
50 μm diameter, density 0.27 g cm^{-3}
ex Fillite.

4. Results and discussion

4.1 Bubble behaviour in response to gravity

Air is less dense than water, therefore the bubble lodges against the top edge of the motionless cylinder. As the cylinder is rotated, the bubble adopts different, stationary positions between the edge and centre of the tube. The bubble is displaced both in the horizontal and vertical planes. As the speed of rotation is increased the bubble moves to the centre (by a diagonal path) where it remains. It is observed that the larger the bubble, the higher the rotation speed required for the bubble to attain the centre. Very small bubbles tend to precess with the liquid about the centre of the cylinder. When an antifoam agent, e.g. Surfynol 104 is added to the water, the air/water interface is rigidified [16] and larger bubbles precess, i.e. > 0.3 mm diameter. Currie and Nieuwkoop [9] found that droplet displacement off axis (both in horizontal and vertical planes) at low rotational speeds was dependent upon the density difference between the two phases and the rotational speed. Although plotting our data on identical axes gave similar results (fig. 3) it did not match Currie and Nieuwkoop's equation:

$$d_v = d_H = \frac{2}{3}\,\frac{g}{\Omega^2}\left(\frac{\varrho - \varrho_o}{\varrho}\right) \tag{15}$$

where: d_V = vertical displacement, d_H = horizontal displacement, ϱ = density of continuous phase, ϱ_o = density of drop or bubble, g = acceleration due to gravity.

From our observations, the position of the bubble appears to depend also, upon bubble size, the interfacial rheology, and viscosity of the surrounding liquid.

Bubble velocity at different angles of inclination (θ) can be predicted by Stokes' law:

$$U = \frac{2gr^2(\varrho - \varrho_o)\sin\theta}{9\,\eta}. \tag{16}$$

The observed bubble velocities in the spinning cylinder are much lower than predicted by Stokes, indicating that drag forces other than the viscous forces are acting upon the bubble (fig. 4).

From bubble velocity measurements (in sodium dodecyl sulphate and sodium oleate solutions) using gravity as the driving force, $\hat{D}$ was plotted against T (fig. 5). These results were compared with the $\hat{D}$ value

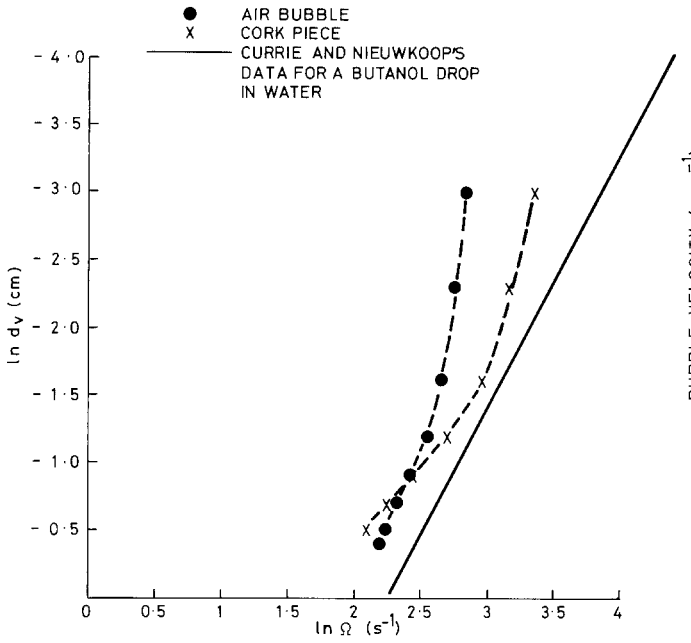

Fig. 3. To show variation of vertical displacement of body from the axis of the rotating tube with angular velocity

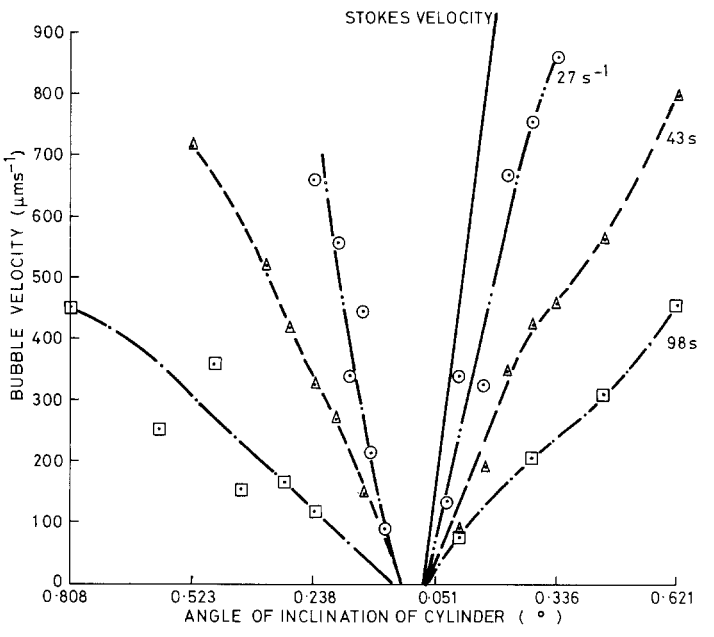

Fig. 4. Bubble velocity vs angle of inclination at three rotational speeds (bubble dia 0.7 mm in distilled water)

expressed as a function of T. Although the data matched the general from of equation (8), a better empirical fit was found to be:

$$\hat{D} = \frac{14\pi + 8T}{8T}. \qquad (17)$$

Bubbles larger than 1.5 mm diameter did not travel smoothly along the axis of the tube but tended to oscillate from side to side. No net movement in response to gravity was observed until the cylinder was inclined at a large angle. Movement was very rapid and the bubble stopped after a short distance (~ 5 mm). Upon increasing the angle of inclination the bubble again moved a short distance. As the speed of rotation was increased, the angle of inclination required for bubble movement became greater.

The flow of liquid within the cylinder was investigated by injecting a hollow resin sphere with potassium permanganate and observing the dye escaping from the sphere during rotation (figs. 6, 7, 8). The dye emerged as a helix and eventually formed a slug ahead of the sphere. The dye did not spread throughout the cylinder by the spinning action, indicating no mixing of the liquid layers. After several minutes the dye column progressed to the end caps and spread slightly within this area. The presence of the slug provides visual evidence of the Taylor column.

4.2 Bubble behaviour in response to an electric field

In this second set of experiments, the cylinder was horizontal i.e. gravity did not effect movement. The velocity of the air bubbles was investigated as a function of rotational speed, bubble size and field strength.

At very low rotational speeds, i.e. before the bubble attained the centre of the cylinder, the observed bubble velocity (80 V, 0.8 mm diameter) increased with increasing rotation speed (fig. 9). The effect is observed quite clearly for distilled water. At 20 s^{-1} the bubble was at the centre of the cylinder and subsequent increases in rotational speed decreased the observed velocity of the bubble. The presence of a surfactant SLS (= sodium dodecyl sulphate) does modify the behaviour: bubble velocity at >30 s^{-1} was too slow to measure accurately.

The effect of bubble diameter upon observed bubble velocity was also affected by the nature of the surfactant. A marked radius dependence emerged, the larger the bubble the higher the velocity (fig. 10).

The variation of velocity with applied voltage was not linear, even after corrections for slight changes in bubble size during the experiment (fig. 11). This is in contrast to observations made in conventional, static electrophoresis cells, where particle velocity is directly proportional to the voltage applied. These results indicate that rotation may have a profound effect upon

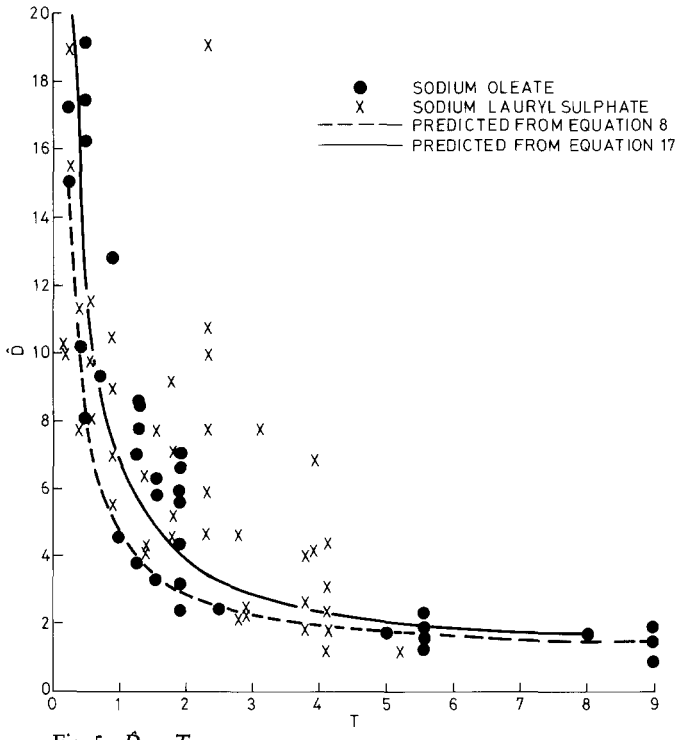

Fig. 5. $\check{D}$ vs T

the double layer, perhaps altering the distortion under different bubble size and rotation velocity regimes. Albeit this reservation, various experiments were performed to measure the mobility of air bubbles in the presence of anionic, cationic, non-ionic and zwitterionic survactants, and at various pH (see figs. 12 and 13). The electrokinetic potential and surface charge density for each air-aqueous condition were calculated using equations (12) and (13) and the results may be found in table 1.

Table 1. Electrokinetic data on air bubbles

system	pH	concentration mol dm^{-3}	surface charge density μ C cm^{-2}	potential mV
distilled water	4		0.9±0.5	− 0.6±0.1
	6		4.1±1.4	−22.5±7.6
	7		4.3±3.4	−74.2±60.0
	9		5.1±1.8	− 8.8±3.1
arquad C/50		10^{-6}	0	0
		10^{-5}	2.8	+ 5.0
		2.5×10^{-5}	1.5	+ 1.7
		5.0×10^{-5}	2.2	+ 1.7
		10^{-4}	2.8	+ 1.5
Sodium dodecyl sulphate		10^{-5}	3.5	− 6.0
		10^{-4}	6.4	− 3.5
NPE 1800		10^{-4}	4.4	− 2.4
empigen BB (impure)		10^{-6}	2.1	−11.5
		10^{-4}	0.9	+ 0.5
potassium chloride	7	10^{-4}	5.3±3.1	− 2.9±1.7
empigen BB (purified)		10^{-4}	5.4±1.3	− 3.0±0.7

Note: Data without error bars are for single determinations.

Overall, the following trends were apparent: in water, potassium choride and anionic surfactant solutions, the air-aqueous interfacial charge is negative. Double distilled water had an uncharacteristically high electrokinetic potential compared with salt solution. This was attributed to the non-rigidity of the clean

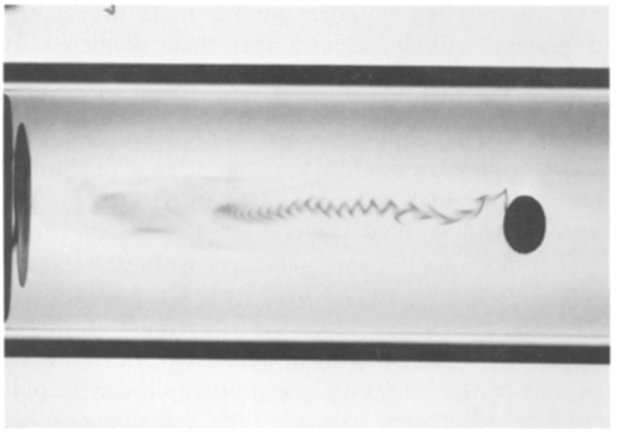

Fig. 6. Showing helix of dye emerging from a spinning, hollow, resin sphere the "Taylor column" can be seen clearly

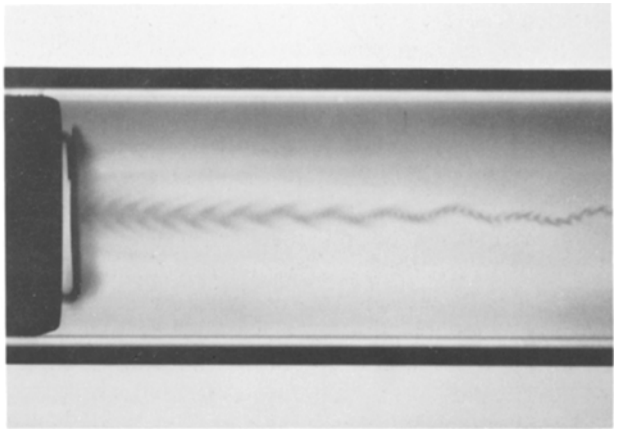

Fig. 7. Showing the slug of dye approaching end-cap/electrode in the spinning cylinder

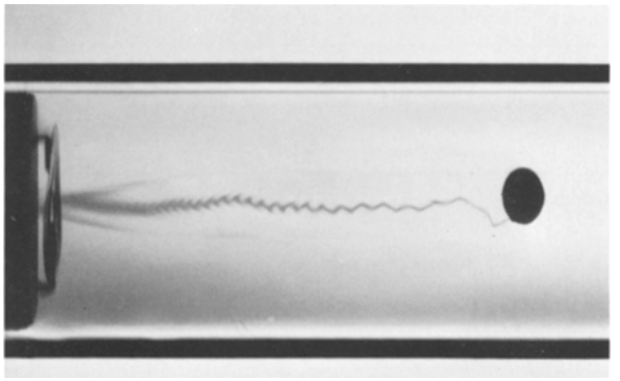

Fig. 8. Showing an overall impression of the flow liquid due to a body inside the spinning cylinder

air-water interface. Consequently, the value of $\hat{D}$, as a function of T, could not be calculated from equation (8). At low pH, air bubbles had a small net negative charge; at alkaline pH, the negative charge was increased. At pH 6, the air bubble charge appeared to be higher than at pH 9, but the ionic strength was low, approaching the distilled water case. A change in the rheology of the air-aqueous interface could, again, explain this result. The surfactant, sodium dodecyl sulphate, was apparently adsorbing at the air-aqueous interface and giving rise to a fairly high surface charge density. However, the double layer is compressed, due to the ionic strength and the potential diminishes away from the interface to approach the electrokinetic potential values obtained for potassium chloride solutions. The pluronic type non-ionic surfactant slightly increased the negative potential. At very low concentration (10^{-6} mol l^{-1}) the cationic surfactant Arquad C/50 rendered the electrokinetic potential zero, but with increasing concentration, this potential became positive. The magnitude of the positive potential declined with increasing surfactant concentration which again is consistent with compression of the double layer at high-ionic strength. The zwitterionic Empigen BB acted in a similar fashion to the cationic, but a concentration of 10^{-4} mol l^{-1} was required for a positive potential. This behaviour was attributed to a cationic precursor contaminant, as upon purification of the surfactant by recrystallisation, the air-aqueous interface remained negatively charged at a concentration of 10^{-4} mol l^{-1}.

The mobility of small, hollow glass spheres was measured in the spinning cylinder. The results were difficult to analyse as the spheres moved in clumps of approximately 250. D, the drag coefficient was calculated for the clump as it was felt that the Taylor column would develop for the whole. The electrokinetic potential, calculated for the individual spheres and for the clump respectively, was between 0 and −11.5 mV. The fillite beads were crushed and the electrokinetic potential measured in the Rank Microelectrophoresis apparatus. ζ was calculated to be 1.4 mV. This value is low compared with values for quartz at pH 7 quoted in the literature (~ 60 mV, [17]), however, it compares favourably with the spinning cylinder data.

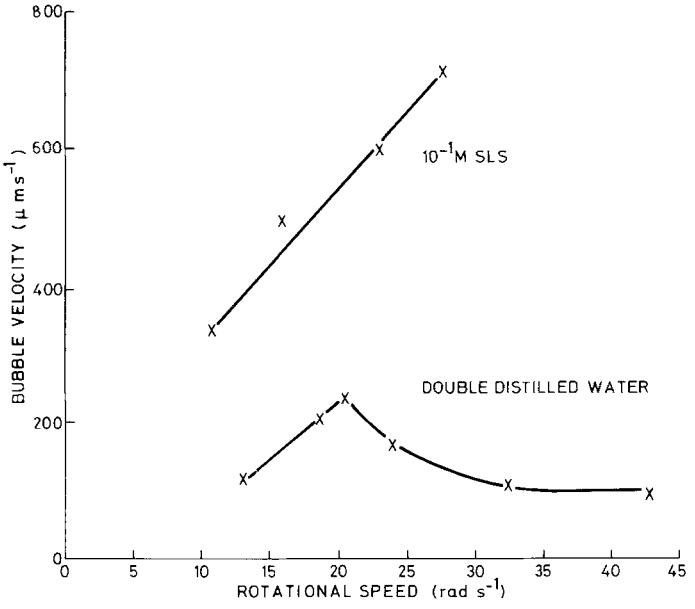

Fig. 9. Bubble velocity vs ritational speed (bubble dia. 0.8 mm, 80 volt)

5. Conclusions

In the spinning cylinder, bubbles move in response to gravity with a velocity less than predicted by Stokes, due to dynamic and viscous drag forces acting upon the bubble. A coefficient describing the drag force has been proposed, which takes into account the Taylor column of liquid which develops at the bubble size and angular velocity regimes chosen for the experiments.

The drag coefficient measured from the results where the bubble moves under the force of gravity, has been used to evaluate the electrophoretic force experienced by the bubble in translatory motion along the axis of the horizontal, spinning cylinder. Bubble mobility differences in magnitude and direction are observed in the presence of a variety of surfactants and over a range of pH values. Assuming that the con-

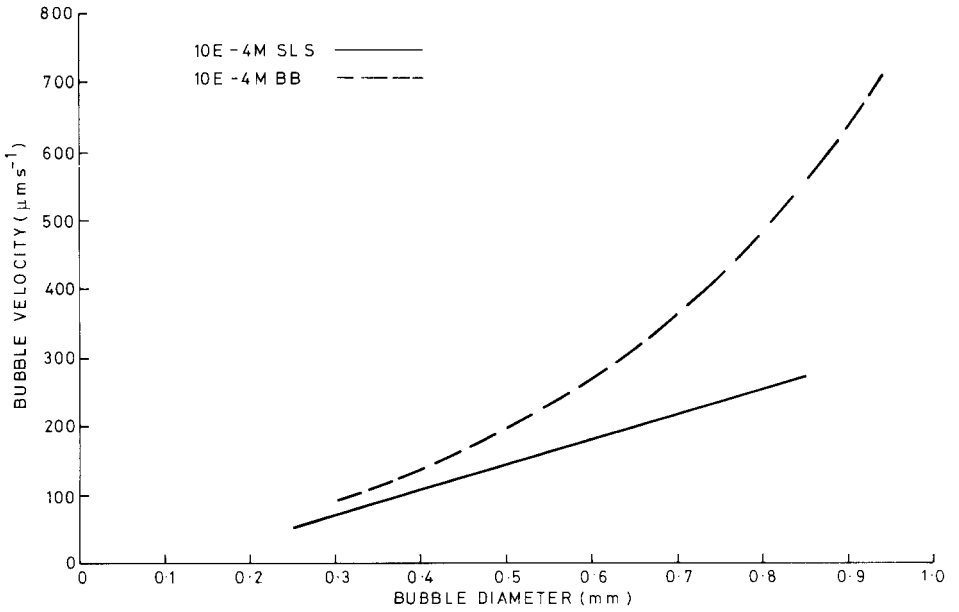

Fig. 10. Bubble velocity vs bubble diameter (80 volt)

tinuity of the double layer is undisturbed by the flow of liquid round the bubble, calculations show zeta potentials of -2 mV for bubbles in potassium chloride solution. Surfactants adsorb at the air-aqueous interface, giving rise to surface charge densities of 5 μC cm^{-2}, and electrokinetic potentials of approximately $2-5$ mV. A surface charge density of this magnitude would normally give rise to a much higher zeta potential, therefore our findings suggest that double layers are indeed disturbed by the spinning of the cell.

The method is sensitive in that it can detect minor impurities in surfactant solutions.

The drag coefficient D cannot be used for bubbles in distilled water, probably due to a change in the rheological properties of the air-aqueous interface.

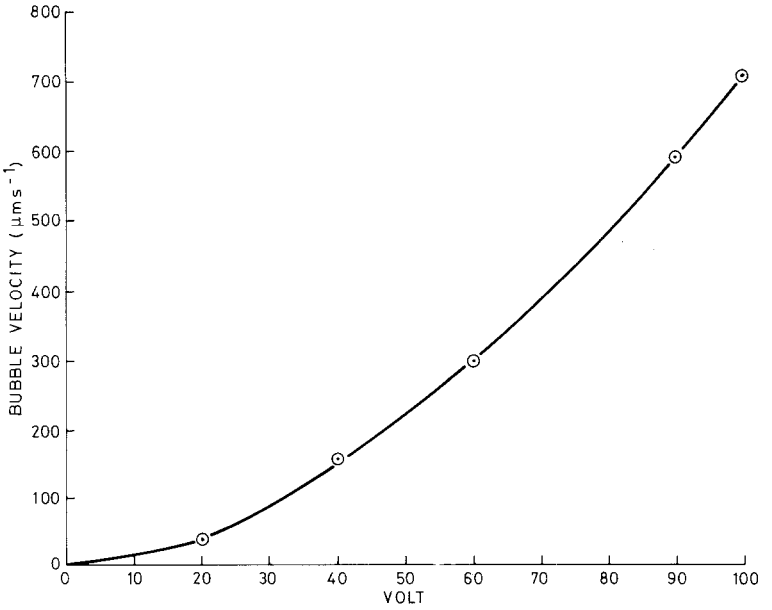

Fig. 11. Bubble velocity vs applied voltage (bubble dia 0.8 mm, rotational speed 25 s^{-1}) in distilled water

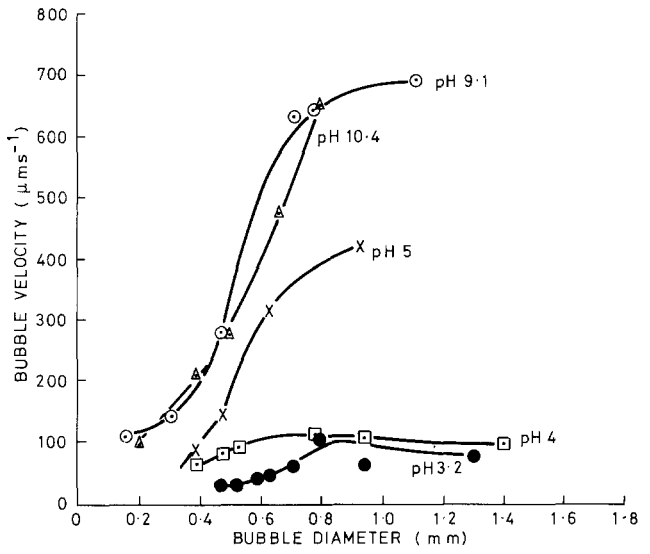

Fig. 12. Bubble velocity vs bubble diameter at different pH (80 volt, 21 s^{-1})

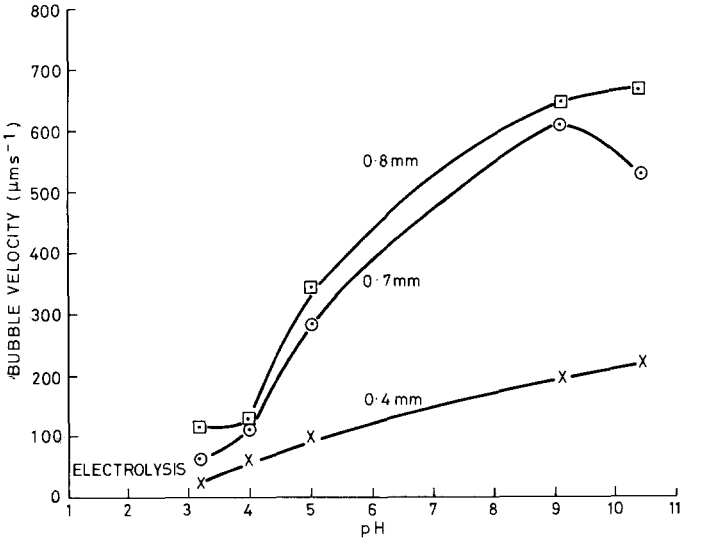

Fig. 13. Bubble velocity vs pH for different bubble sizes (80 volt, 21 s^{-1})

Further work is required to determine the drag coefficient for a range of interfacial rheological conditions.

Acknowledgements

We would like to thank Dr. A. L. Smith and Dr. R. W. Huddleston for their help and advice on the method, apparatus and theory involved with the work. We are also indebted to Professor G. K. Batchelor FRS and Dr. J. Rallison for useful discussions concerning the hydrodynamics of the situation.

We would like to thank the Directors of BP international plc for permission to publish this paper.

References

1. Usui, S., H. Sasaki, H. Matsukawa, J. Colloid and Interface Science **81**, 80 (1981).
2. Collins, G. L., M. Motarjemi, G. J. Jameson, J. Colloid and Interface Science **63**, 69 (1978).
3. Whybrew, W. E, G. D. Kuizer, R. Gunn, J. Geophysical Research **57**, 459 (1952).
4. Huddleston, R. W., A. L. Smith, Int. Foams Conference, Brunel University (1975).
5. Stewartson, K., Proc. Camb. Phil SOC **48**, 168 (1952).
6. Hocking, L. M., D. W. Moore, I. C. Walton, J. Fluid Mechanics **90**, 781 (1970).
7. Batchelor, G. K., An introduction to fluid mechanics, Cambridge University Press (1967).
8. Taylor, A. J., F. W. Wood, Trans. Faraday Society **53**, 523 (1957).
9. Currie, P. K., J. van Nieuwkoop, J. Colloid and Interface Science **87**, 301 (1982).
10. Rallison, J., Private Communication (October 1981).
11. Levich, B. V. G., 'Physico-chemical Hydrodynamics', Prentice Hall Inc. (1962).
12. Hunter, R. J., 'Zeta Potential in Colloid Science', Academic Press, London (1981).
13. Davies and Rideal, 'Interfacial Phenomena', Academic Press, London (1961).
14. Debye, P., E. Hückel, Physik Z. **24**, 185 (1923).
15. Huddleston, R. W., PhD Thesis (February 1974).
16. McShea and Callaghan, unpublished results.
17. Fuerstenau, D. W., Pure and Applied Chemistry **24** (1), (1970).
18. Hippel, T., H. Brenner, Low Reynolds Number Hydrodynamics and its Application, Sijthoff and Nordhoff, (1975).
19. Moore, D. W., T. G. Saffman, Phil. Trans. Roy. Soc. **264**, 597 (1969).

Received January 17, 1983;
accepted May 9, 1983

Authors' address:

Julie A. McShea
BP Research Centre
Sunbury-on-Thames
Middlesex TW16 7LN (U.K.)